CrystEngComm

ROYAL SOCIETY OF CHEMISTRY

COMMUNICATION

Cite this: *CrystEngComm*, 2022, **24**, 5557

Received 8th June 2022,
Accepted 17th July 2022

DOI: 10.1039/d2ce00791f

rsc.li/crystengcomm

A micron-sized Co-MOF sheet to activate peroxymonosulfate for efficient organic pollutant degradation†

Fu-Xue Wang,[ab] Zi-Chen Zhang,[ab] Xiao-Hong Yi,[ab] Chong-Chen Wang,[*ab] Peng Wang,[ab] Chao-Yang Wang[ab] and Baoyi Yu[c]

A Co-MOF with a 2D morphology (BUC-92) was prepared, which exhibited outstanding rhodamine B (RhB) degradation performance *via* peroxymonosulfate (PMS) activation. RhB was degraded completely within 10 min in the presence of 0.2 g L^{-1} BUC-92 and 0.2 mM PMS, much higher than that using our previously reported MOF BUC-67 (54.4%) under the same conditions, whose composition was similar to that of BUC-92. A related mechanism was proposed. A fixed bed reactor was built to further evaluate the potential application of BUC-92.

Recently, advanced oxidation processes (AOPs), especially the persulfate (PS)-based advanced oxidation process (PS-AOP), have become hotspots in water treatment, which can efficiently degrade organic pollutants by the formed reactive oxygen species (ROSs), high-valent metal species or direct electron transfer from organic pollutants to PS.[1] It was found that some transition metals like Fe^{2+}, Mn^{2+} and Cu^{2+} could be used for PS activation, but they are not comparable with Co^{2+}.[2,3] Therefore, Co-based heterogeneous catalysts receive wide attention.

Metal–organic frameworks (MOFs) consisting of metal ions/clusters and organic ligands have attracted increasing attention in recent years due to their interesting structures and charming properties, as well as potential applications.[4,5] To date, various applications of MOFs have been researched, including but not limited to CO_2 capture,[6,7] catalysis/photocatalysis,[8–10] adsorption,[11] drug delivery,[12–14] electrochemistry,[15–17] fluorescent detection[18,19] and so on.[20–23] Many researchers once focused on MOFs with morphologies of 0D particles and 1D nanorods/nanowires.[24] Recently, increasing efforts have been devoted to 2D MOFs due to their large potential in catalysis, separation and sensing.[24–26] Taking catalysts for example, more accessible active sites on the surface and faster mass transfer can be accomplished over 2D MOFs, which promote their catalytic performances.[27] Besides, the 2D morphology was considered to be suited for the formation of membranes due to the increase in both the adhesion and contact area between the MOFs and the substrates.[25]

Herein, a new Co-based MOF namely BUC-92 with a 2D morphology (Fig. 1c) was synthesized by a solvothermal reaction between $CoCl_2{\cdot}6H_2O$ and *cis*-1,3-dibenzyl-2-imidazolidone-4,5-dicarboxylic acid (H_2L). The crystal structure analyses revealed that the six-coordinated Co^{2+} is linked by one nitrogen atom (N1) from L^{2-}, two oxygen atoms (O2 and O4) from two different carboxylate groups of the same L^{2-}, one oxygen atom (O1) from the adjoining L^{2-} and two oxygen atoms from two coordinated water molecules (Fig. 1a). The Co^{2+} ions are linked into one-dimension chains by L^{2-} ligands along the *b*-axis (Fig. 1b). The Co–O distances of BUC-92 are in the range of 2.042 (3)–2.117 (4) Å, comparable to those of BUC-67 (2.074 (4)–2.110 (5) Å), a previously reported Co-MOF linked by L^{2-} and bpy (bpy = 4,4-bipyridine).[28] The Co–N bond length of BUC-92 was 2.317 (3) Å, longer than those in BUC-67 (2.176 (5) to 2.191 (6) Å).[28] The bond lengths and angles of BUC-92 could be found in Table S1.† Crystal data of BUC-92 (M_r = 447.30 g mol^{-1}): orthorhombic system, space group *Pbca*, a = 10.0404 (8) Å, b = 9.9260 (7) Å, c = 38.902 (3) Å, V = 3877.0 (5) $Å^3$, Z = 8, T = 293 K, μ(MoKα) = 0.93 mm^{-1}, D_c = 1.330 g cm^{-3}, total reflections 5528, unique reflections 3646, R_{int} = 0.065, F(000) = 1848, GOF on F^2: 1.044, R_1/wR_2 ($I > 2\sigma(I)$): 0.0736/0.1745, R_1/wR_2 (all data): 0.1231/0.1949.

[a] *Beijing Key Laboratory of Functional Materials for Building Structure and Environment Remediation, Beijing University of Civil Engineering and Architecture, Beijing 100044, PR China. E-mail: wangchongchen@bucea.edu.cn, chongchenwang@126.com*

[b] *Beijing Energy Conservation & Sustainable Urban and Rural Development Provincial, and Ministry Co-construction Collaboration Innovation Center, Beijing University of Civil Engineering and Architecture, Beijing 100044, PR China*

[c] *Key Laboratory of Urban Agriculture (North China), Ministry of Agriculture, College of Biological Sciences Engineering, Beijing University of Agriculture, Beijing 102206, China*

† Electronic supplementary information (ESI) available: Extra experimental details, FTIR, TGA and crystallographic data. CCDC 2172782. For ESI and crystallographic data in CIF or other electronic format see DOI: https://doi.org/10.1039/d2ce00791f

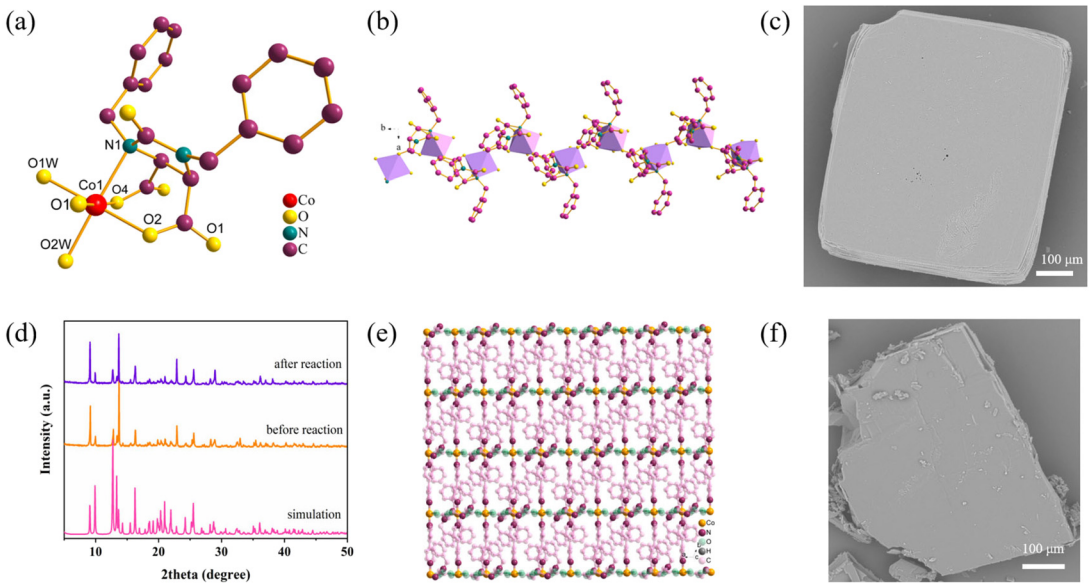

Fig. 1 (a) Asymmetric unit of BUC-92 (H atoms were omitted). (b) 1D chain structure of BUC-92. (c) SEM image of BUC-92, (d) XRD of BUC-92. (e) The packing view of BUC-67. Reprinted with permission from ref. 28 copyright 2018 Elsevier. (f) SEM image of BUC-67.

The powder XRD patterns of the as-synthesized BUC-92 fitted well with the simulated ones from the CIF file (CCDC number: 2172782), indicating the high crystallinity and purity of the BUC-92 powder (Fig. 1d). The original morphologies of BUC-92 and BUC-67 were observed using the scanning electronic microscopy (SEM) images. As displayed in Fig. 1c and f and S1a and b,† both BUC-92 and BUC-67 were 2D sheets with sizes of *ca.* 600 μm length, *ca.* 550 μm width and *ca.* 50 μm thick. The uniform distribution of various elements of BUC-92 could be observed by energy dispersive X-ray spectroscopy (EDS) elemental mapping (Fig. S1†). The contents of C, N, O and H in BUC-92 measured by CNHO element analyses were 50.9%, 6.5%, 25.6% and 4.4%, respectively, matching well with the calculated values based on $C_{19}H_{20}CoN_2O_7$ (C 51.0%, N 6.3%, O 25.0%, and H 4.5%). The thermal stability of BUC-92 was tested by TGA, indicating that the structure was stable up to 298 °C (Fig. S2†). The coordinated water molecules were lost at 125–200 °C.

The PS-AOP catalytic performances of BUC-92 and BUC-67 were evaluated based on rhodamine B (RhB) degradation *via* peroxymonosulfate (PMS) activation under dark conditions. As illustrated in Fig. 2a, only *ca.* 5% RhB was degraded in the control experiments of PMS, BUC-92 and BUC-67 systems after 20 min, respectively. In the presence of both BUC-67 and PMS, RhB removal efficiency was increased to 54.5% within 10 min, higher than that by the homogeneous PMS activation *via* completely dissolved Co^{2+} (49.8%). In comparison, RhB could be completely degraded over BUC-92 under identical conditions, which was comparable to some reported counterpart Co-based catalysts (Table S2†). The reaction rate (k) fitted by pseudo-first-order kinetics ($-\ln[C/C_0] = kt$) for RhB degradation was 0.3249 min^{-1} over BUC-92, which was 2.58 times as high as that over BUC-67 (0.126 min^{-1}). The catalytic performance of BUC-92 and BUC-67 remained for at least five reuse cycles of experiments (Fig. S3†). After catalytic RhB degradation *via* PMS activation, no obvious change could be found from the XRD results of both BUC-92 and BUC-67 (Fig. 1d and S4†). The leaching Co ion was less than 2.2 mg L^{-1} during PMS activation at pH 3.0–9.0 (Fig. S5–S7†), suggesting good stability. Moreover, the morphologies showed no change after catalytic RhB degradation *via* the PS-AOP (Fig. S8†).

PS-AOPs are usually affected by solution pH, since it might change the surface charge of the catalysts and the form of the organic pollutants, as well as influence the redox

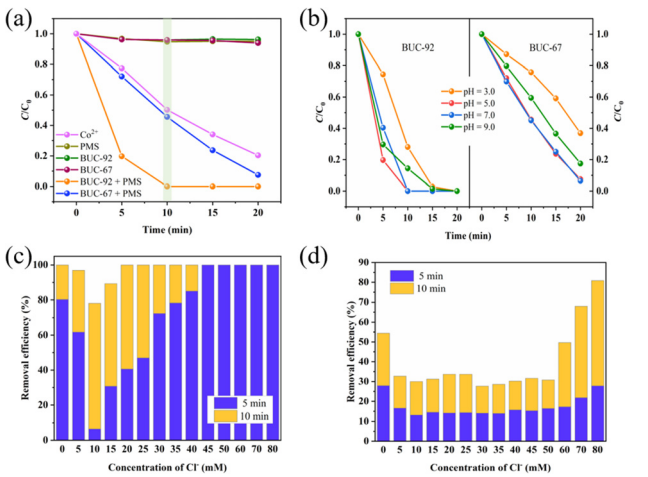

Fig. 2 (a) RhB degradation performances over BUC-92 and BUC-67 under different conditions. (b) Influences of initial pH on RhB removal efficiencies over BUC-92 and BUC-67. Influences of Cl^- on RhB removal efficiencies over (c) BUC-92 and (d) BUC-67. Reaction conditions: 200 mg L^{-1} catalyst (2.0 mg L^{-1} dissolved Co^{2+} ion in the homogeneous system), 0.2 mM PMS, 50 mL 10 mg L^{-1} RhB, in the dark.

potential of ROSs.[27] The initial pH value of RhB solution was adjusted from 3.0 to 9.0, as depicted in Fig. 2b. 78.0% and 85.6% of RhB were degraded over BUC-92 within 10 min at pH 3.0 and 9.0, respectively. However, the RhB removal efficiencies were only 24.3% and 40.6% over BUC-67 under the same conditions. At near neutral pH (5.0–7.0), 100% of RhB could be decomposed over BUC-92 within 10 min, much higher than that over BUC-67 (54.5%). These results indicated that the neutral conditions were beneficial for the reaction, which was consistent with previous reports.[29]

It was deemed that PS-AOPs were greatly affected by inorganic ions, especially HCO_3^- and Cl^-.[30,31] Herein, the influences of HCO_3^- and Cl^- on RhB degradation were studied. As showed in Fig. S9,† RhB removal efficiencies declined from 100% and 92.5% with the absence of HCO_3^- to 55.0% and 62.2% over BUC-92 and BUC-67 within 20 min in the presence of 5 mM HCO_3^-, respectively. Moreover, the removal efficiencies were reduced by 85.1% and 88.7% over BUC-92 and BUC-67, as the HCO_3^- concentration increased to 50 mM, respectively. The pH values of the RhB solution before and after the addition of 50 mM bicarbonate were 5.0 and 7.6, respectively. It can be found that RhB was completely degraded even at pH = 9.0 (Fig. 2b). Therefore, the negative effect of bicarbonate on RhB degradation might not result from the change of the pH, but attributed to the consumption of ROSs by HCO_3^-.[29]

It was reported that the effects of the co-existing Cl^- on the PS-AOP might be negative or positive, which depended on its concentration and the pH value of solution.[32] In order to reveal the influences of Cl^- on RhB removal efficiencies over BUC-92 and BUC-67, the reactions were carried out in the presence of 5–80 mM Cl^-. As illustrated in Fig. 2c, Cl^- might reduce the RhB degradation efficiency over BUC-92 in a range of 5–35 mM Cl^- in the first 5 min. However, 100% RhB was degraded within only 5 min when the Cl^- concentration increased to 45–80 mM. Similarly, the degradation efficiency over BUC-67 was inhibited at low Cl^- concentration (5–50 mM), whereas it was obviously promoted at high Cl^- concentration (70–80 mM) (Fig. 2d). It could be attributed to the low-concentration Cl^- that would prefer to consume $^{\cdot}SO_4^-$, while it could directly react with PMS at high concentration to form Cl_2 or HClO to promote the degradation of organic pollutants.[30,32,33]

To clarify the RhB degradation mechanism over BUC-92 and BUC-67, ROS capture experiments were conducted. It was known that $^{\cdot}SO_4^-$, $^{\cdot}OH$ and nonradical species $^1O_2$ could be formed to attach organic pollutants *via* the PS-AOP. Herein, three common candidates, ethanol (EtOH), *tert*-butyl alcohol (TBA) and L-histidine were used to test whether these ROSs were involved in the system. EtOH can react with both $^{\cdot}SO_4^-$ (k = 1.6–7.7 × 10^7 M^{-1} s^{-1}) and $^{\cdot}OH$ (k = 1.2–2.8 × 10^9 M^{-1} s^{-1}), while TBA only quenches $^{\cdot}OH$ (k = 3.8–7.6 × 10^8 M^{-1} s^{-1}).[34] L-Histidine could scavenge $^1O_2$ (k = 3.2 × 10^7 M^{-1} s^{-1}).[35] As demonstrated in Fig. 3a, the RhB degradation over BUC-92 slightly decreased when 500 mM TBA or 500 mM EtOH was added, whereas it was reduced by 75.9% in 20 min and the

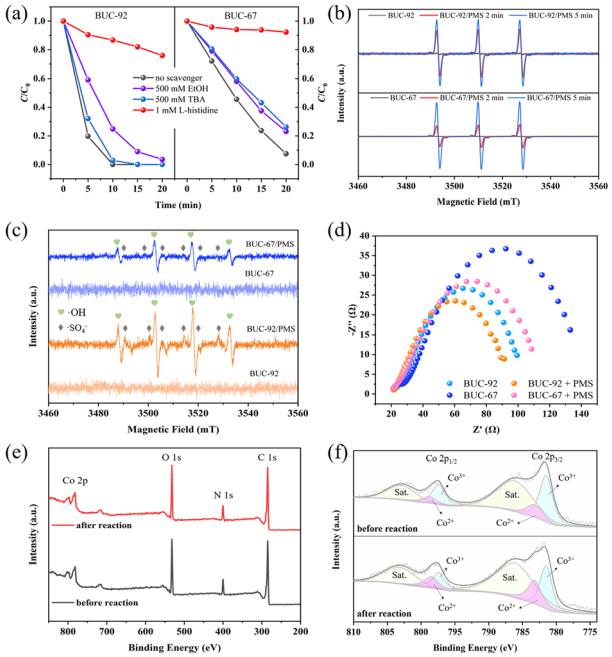

Fig. 3 (a) Effects of different scavengers on RhB degradation over BUC-92 and BUC-67. ESR spectra of (b) TEMP–$^1O_2$ and (c) DMPO–$^{\cdot}SO_4^-$ and DMPO–$^{\cdot}OH$ over BUC-92 and BUC-67. (d) Electrochemical impedance spectroscopy of BUC-92 and BUC-67 with/without PMS. (e) XPS survey spectra of BUC-92. (f) High-resolution XPS spectra of Co 2p in BUC-92 before and after the reaction.

degradation rate decreased from 0.3249 min^{-1} to 0.013 min^{-1} in the presence of 1 mM L-histidine. Similar results could be found in the BUC-67/PMS system. Upon the addition of excess TBA or EtOH, the RhB degradation was only decreased by 15.6% within 20 min. In contrast, a strong inhibiting effect on RhB degradation was observed when L-histidine was added. RhB degradation was significantly reduced by 84.8% within 20 min, and the degradation rate declined from 0.126 min^{-1} under initial conditions to 0.0036 min^{-1} in the presence of 1 mM L-histidine. These results suggested that all the three ROSs were generated during the PMS activation, in which the nonradical $^1O_2$ rather than $^{\cdot}SO_4^-$ and $^{\cdot}OH$ dominated the RhB degradation in both BUC-92/PMS and BUC-67/PMS systems.

Furthermore, the formation of the three ROSs in both BUC-92/PMS and BUC-67/PMS systems was directly confirmed by electron spin resonance (ESR) technology. Obviously, there was no characteristic signal in the BUC-92 system or BUC-67 system, whereas triple peaks could be found after addition of PMS (Fig. 3b). The intensity ratio of 1 : 1 : 1 triple peaks were assigned to the TEMP–$^1O_2$ from the combination of 2,2,6,6-tetramethylpiperidine (TEMP) and the formed $^1O_2$,[36] and the intensity of the peaks increased gradually with time. Similarly, no characteristic signal could be found in the presence of a catalyst and 5,5-dimethylpyrroline (DMPO) (Fig. 3c). After the addition of PMS, the characteristic peaks of DMPO–$^{\cdot}SO_4^-$ and DMPO–$^{\cdot}OH$ were observed in both BUC-92/PMS and BUC-67/PMS

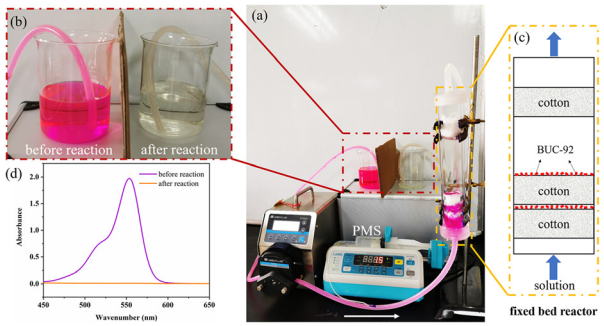

Fig. 4 (a) Photo image of the fixed bed reactor for RhB degradation over BUC-92 *via* PMS activation. (b) Photo image of the RhB solution before and after the reaction. (c) Schematic illustration of the fixed bed reactor. (d) UV-vis absorption spectra of the RhB solution before and after the reaction.

systems, confirming the generation of $^{\bullet}SO_4^-$ and $^{\bullet}OH$. These results revealed that nonradical species $^1O_2$ along with $^{\bullet}SO_4^-$ and $^{\bullet}OH$ were generated during the PMS activation.

In fact, it wasn't a surprise to observe that the generated ROSs were the same in the BUC-92/PMS and BUC-67/PMS systems, because their composites were very similar. What aroused our interest was the organic pollutant removal efficiency over BUC-92 being significantly higher than that over BUC-67. Electrochemical impedance spectroscopy (EIS) of BUC-92 and BUC-67 measured under identical conditions provided solid information to clarify their difference. As illustrated in Fig. 3d, the radius of the circular arc of BUC-92 was much smaller than that of BUC-67 before/after the addition of PMS, indicating a smaller charge transfer resistance of BUC-92. Therefore, BUC-92 showed a faster reaction rate. Besides, more Co^{2+} leached from BUC-92 (2.0 mg L^{-1}) than that from BUC-67 (0.9 mg L^{-1}) (Fig. S6†) into the solution, which might also accelerate the RhB degradation *via* homogeneous catalysis.

The addition of PMS could not only decrease the radius of the catalysts, but also accelerate the electron transfer. As shown in Fig. S10,† obvious current response could be seen from the linear sweep voltammetry (LSV) curves after the addition of PMS. A similar result was found in PMS activation by metal sulfide material.[37]

X-ray photoelectron spectroscopy (XPS) was used to measure the elements and the oxidation state of Co ions in BUC-92 before and after the reaction (Fig. 3e and f and S11†). The Co 2p peak contains a spin doublet ($2p_{3/2}$ and $2p_{1/2}$) of Co^{3+} at 781.5 and 797.4 eV and a doublet for Co^{2+} at 783.2 and 798.7 eV, as well as satellite peaks (Sat.) at 786.1 and 802.92 eV.[36] The Co^{2+}/Co^{3+} ratio increased from 0.32 in the fresh sample to 0.76 after the reaction. The increase of the Co^{2+} content after the reaction was attributed to the charge transfer from PMS to the Co^{3+}, whereas PMS was oxidized to generate $^1O_2$ (eqn (1) and (2)).[38]

$$HSO_5^- \rightarrow SO_5^{\bullet-} + H^+ + e^- \quad (1)$$

$$SO_5^{\bullet-} + SO_5^{\bullet-} \rightarrow {}^1O_2 + 2SO_4^{2-} \quad (2)$$

Considering the excellent catalytic performance and the large size of the BUC-92 sheets, a simple fixed bed reactor was built. The BUC-92 sheets were added into an acrylic tube (D = 24 mm), whose channel was blocked by commercial cotton. The great advantage of the simple reactor was that the catalyst was kept in the reactor without any loss of active sites. The RhB solution (10 mg L^{-1}, 10 mL min^{-1}) and PMS (50 mM, 1.5 mL h^{-1}) were injected into the reactor using a peristaltic pump and a syringe, respectively, as displayed in Fig. 4. It could be found that the pink solution became colourless quickly in the fixed bed reactor, and the RhB concentration decreased from 10 to 0 mg L^{-1}, showing huge potential of BUC-92 towards RhB degradation *via* SR-AOPs.

In conclusion, a Co-MOF BUC-92 with a 2D morphology was synthesized, which exhibited excellent performance for organic pollutant degradation *via* PMS activation in the dark. RhB was completely degraded in the presence of BUC-92 and PMS, in which $^1O_2$ was the major ROS for both BUC-92 and BUC-67 in RhB degradation. The higher catalytic performance of BUC-92 was attributed to faster charge transfer. Furthermore, BUC-92 was used in the fixed bed reactor to quickly degrade RhB in water. This work is expected to offer some important information about Co-based 2D MOFs in catalysis.

Author contributions

Fu-Xue Wang: data curation, investigation, visualization, and writing – original draft. Zi-Chen Zhang: data curation and investigation. Xiao-Hong Yi: data curation. Chong-Chen Wang: conceptualization, funding acquisition, supervision, project administration, and writing – review & editing. Peng Wang: resources. Chao-Yang Wang: software. Baoyi Yu: software.

Conflicts of interest

There are no conflicts to declare.

Acknowledgements

This work was supported by the National Natural Science Foundation of China (51878023), the Beijing Talent Project (2020A27), the Science and Technology General Project of Beijing Municipal Education Commission (KM202110016010), the Young Teachers' Research Ability Enhancement Program for Beijing University of Civil Engineering and Architecture (X21085) and the BUCEA Post Graduate Innovation Project (2021).

References

1 W. Ren, C. Cheng, P. Shao, X. Luo, H. Zhang, S. Wang and X. Duan, *Environ. Sci. Technol.*, 2022, **56**, 78–97.
2 S. He, Y. Chen, X. Li, L. Zeng and M. Zhu, *ACS ES&T Eng.*, 2022, **2**, 527–546.

3 Y. Gao, T. Wu, C. Yang, C. Ma, Z. Zhao, Z. Wu, S. Cao, W. Geng, Y. Wang, Y. Yao, Y. Zhang and C. Cheng, *Angew. Chem., Int. Ed.*, 2021, **60**, 22513–22521.

4 H. Fu, C.-C. Wang and W. Liu, *Chin. Chem. Lett.*, 2022, **33**, 1647–1649.

5 X. Du, S. Wang, F. Ye and Z. Qingrui, *Environ. Res.*, 2022, **206**, 112414.

6 M. Ding, R. W. Flaig, H.-L. Jiang and O. M. Yaghi, *Chem. Soc. Rev.*, 2019, **48**, 2783–2828.

7 Y. Chen, H. Wu, Q. Xiao, D. Lv, F. Li, Z. Li and Q. Xia, *CrystEngComm*, 2019, **21**, 165–171.

8 C. I. Ezugwu, J. M. Sonawane and R. Rosal, *Sep. Purif. Technol.*, 2022, **284**, 120246.

9 Q. Zhao, C.-C. Wang and P. Wang, *Chin. Chem. Lett.*, 2022, DOI: **10.1016/j.cclet.2022.01.033**.

10 C.-C. Wang, X. Ren, P. Wang and C. Chang, *Chemosphere*, 2022, **303**, 134949.

11 Y.-H. Li, C.-C. Wang, X. Zeng, X.-Z. Sun, C. Zhao, H. Fu and P. Wang, *Chem. Eng. J.*, 2022, **442**, 136276.

12 X. Gao, Y. Wang, G. Ji, R. Cui and Z. Liu, *CrystEngComm*, 2018, **20**, 1087–1093.

13 S. Mallakpour, E. Nikkhoo and C. M. Hussain, *Coord. Chem. Rev.*, 2022, **451**, 214262.

14 I. Abánades Lázaro, C. J. R. Wells and R. S. Forgan, *Angew. Chem., Int. Ed.*, 2020, **59**, 5211–5217.

15 J. Wang, K. O. Kirlikovali, S. Y. Kim, D.-W. Kim, R. S. Varma, H. W. Jang, O. K. Farha and M. Shokouhimehr, *CrystEngComm*, 2022, **24**, 2925–2947.

16 B. Zhang, Y. Zheng, T. Ma, C. Yang, Y. Peng, Z. Zhou, M. Zhou, S. Li, Y. Wang and C. Cheng, *Adv. Mater.*, 2021, **33**, 2006042.

17 J. M. Gonçalves, P. R. Martins, D. P. Rocha, T. A. Matias, M. S. S. Julião, R. A. A. Munoz and L. Angnes, *J. Mater. Chem. C*, 2021, **9**, 8718–8745.

18 S. Nandi, M. Sk and S. Biswas, *Dalton Trans.*, 2020, **49**, 12565–12573.

19 A. Das, S. Ghosh, L. Bourda, M. Sk, K. Banerjee, K. Van Hecke and S. Biswas, *CrystEngComm*, 2022, **24**, 4723–4730.

20 X. Qiu, L. Liu, W. Xu, C. Chen, M. Li, Y. Shi, X. Wu, K. Chen and C. Wang, *Antioxidants*, 2022, **11**, 945.

21 F.-X. Wang, C.-C. Wang, P. Wang and B.-C. Xing, *Chin. J. Inorg. Chem.*, 2017, **33**, 713–737.

22 Y. Shi, X. Rong, C. Chen, M. Wu, Y. Takai, X. Qiu, C. C. Wang, Y. Shimasaki and Y. Oshima, *J. Fac. Agric., Kyushu Univ.*, 2021, **66**, 211–216.

23 C.-Y. Wang, L. Ma, C.-C. Wang, P. Wang, L. Gutierrez and W. Zheng, *Environmental Functional Materials*, 2022, **1**(1), 49–66.

24 M. Zhao, Y. Huang, Y. Peng, Z. Huang, Q. Ma and H. Zhang, *Chem. Soc. Rev.*, 2018, **47**, 6267–6295.

25 A. Dhakshinamoorthy, A. M. Asiri and H. Garcia, *Adv. Mater.*, 2019, **31**, 1900617.

26 Y. Pan, R. Abazari, J. Yao and J. Gao, *JPhys Energy*, 2021, **3**, 032010.

27 F.-X. Wang, C.-C. Wang, X. Du, Y. Li, F. Wang and P. Wang, *Chem. Eng. J.*, 2022, **429**, 132495.

28 X.-H. Yi, F.-X. Wang, X.-D. Du, H. Fu and C.-C. Wang, *Polyhedron*, 2018, **152**, 216–224.

29 C. Xiao, M. Zhang, C. Wang, X. Yan, H. Zhang, S. Chen, Y. Yao, J. Qi, S. Zhang and J. Li, *Chem. Eng. J.*, 2022, **444**, 136385.

30 J. Yan, J. Li, J. Peng, H. Zhang, Y. Zhang and B. Lai, *Chem. Eng. J.*, 2019, **359**, 1097–1110.

31 X.-W. Zhang, F. Wang, C.-C. Wang, P. Wang, H. Fu and C. Zhao, *Chem. Eng. J.*, 2021, **426**, 131927.

32 Y. Liu, B. Yang, Q. Li, L. Ma, L. Li and M. Chen, *Huanjing Gongcheng Xuebao*, 2021, **15**, 1487–1499.

33 Y. Xue, Z. Wang, R. Naidu, R. Bush, F. Yang, J. Liu and M. Huang, *Chem. Eng. J.*, 2022, **433**, 134546.

34 T. Zeng, X. Zhang, S. Wang, H. Niu and Y. Cai, *Environ. Sci. Technol.*, 2015, **49**, 2350–2357.

35 Y. Wang, D. Cao and X. Zhao, *Chem. Eng. J.*, 2017, **328**, 1112–1121.

36 Q. Wang, J. Lu, Y. Jiang, S. Yang, Y. Yang and Z. Wang, *Chem. Eng. J.*, 2022, **443**, 136483.

37 F. Wang, H. Fu, F.-X. Wang, X.-W. Zhang, P. Wang, C. Zhao and C.-C. Wang, *J. Hazard. Mater.*, 2022, **423**, 126998.

38 X. Mi, P. Wang, S. Xu, L. Su, H. Zhong, H. Wang, Y. Li and S. Zhan, *Angew. Chem., Int. Ed.*, 2021, **60**, 4588–4593.